Quasiparticle properties of a coupled two-dimensional electron-phonon system

R. Jalabert* and S. Das Sarma
Department of Physics and Astronomy, University of Maryland, College Park, Maryland 20742
(Received 24 April 1989)

We calculate quasiparticle properties of a weakly polar two-dimensional electron gas by taking into account both electron-electron Coulomb and electron–optical-phonon Fröhlich interactions. Electronic self-energy is calculated exactly in the leading order of the total effective dynamical interaction. The total effective dynamical interaction is obtained within the random-phase approximation (RPA) by starting from the total bare interaction, which includes both Coulomb and Fröhlich interactions and then by screening it with all the bubble diagrams. Our theory thus treats Coulomb and Fröhlich interactions on an equal footing and includes all effects (within the RPA) of Fermi statistics, Landau damping, plasmon-phonon mode coupling, phonon self-energy correction, and dynamical screening. We include finite-thickness effects in actual GaAs-based semiconductor microstructures by considering electron- and phonon- ("slab modes") confinement effects. Some of our interesting results are (1) Coulomb and Fröhlich interaction effects are nonmultiplicative, and the actual many-body correction for an electron gas is substantially different from the one-polaron result; (2) there are interesting and observable plasmon- and phonon-induced satellite structures in the low-energy side of the electronic spectral function and the density of states; (3) at low electron densities phonons tend to screen Coulomb interaction, whereas at large electron densities electrons screen the Fröhlich interactions; (4) our calculated effective mass and inelastic-scattering length are consistent with the available experimental results.

I. INTRODUCTION

Artificially made semiconductor microstructures (heterojunctions and quantum wells) constitute ideal systems for two-dimensional (2D) electron confinement[1] and have been extensively studied during recent years because of their fundamental and technological interest. The modulation-doping technique allows spatial separation of the ionized impurities from the conduction electrons through the growth of an undoped spacer layer, giving rise to a very pure two-dimensional electron gas (2D EG) with extremely high mobilities. The reduced effect of the impurities makes the 2D EG more suitable than the 3D EG for the study of many-body effects. In spite of this, there have not been studies of electron-electron interaction effects in the 2D EG which are as complete as those in the 3D EG.[2] One of the objectives of this paper is to provide, within the leading-order perturbation theory, a fairly complete study of 2D quasiparticle properties. We analyze the electron-electron interaction in the 2D EG within the framework of the random-phase approximation (RPA) and find important departures from the noninteracting 2D EG and the corresponding results in the 3D EG.

Since the 2D semiconductor microstructures are made of polar III-V or II-VI semiconductor materials the carriers interact with the longitudinal-optical (LO) phonons via the long-range Fröhlich interaction. The electron-phonon interaction affects many of the electronic physical properties such as effective mass, inelastic (or phase-breaking) carrier lifetime, density of states, etc., and these have recently attracted considerable experimental[3–5] and theoretical[6,7] attention. Most of the theoretical studies have been carried out in the one-electron approximation (the so-called single-polaron limit) or including screening via *ad hoc* approximations (involving mostly static screening). This is in sharp contrast to the real situation, where one has a finite electron density with the electron Fermi and plasma energies being comparable to the LO-phonon energy. A second objective of this paper is a fairly comprehensive study of the coupled electron–LO-phonon problem for two-dimensional systems. Electron-electron and electron-phonon interactions are treated on an equal footing, our only approximations being the use of the RPA and the neglect of vertex corrections. We find that even in the weak-electron-phonon-coupling limit the electronic properties can be substantially modified by the Fröhlich interaction, and, conversely, that the measurement of phonon-related effects is greatly affected by the Coulomb interaction between the electrons. So, Coulomb and Fröhlich interactions cannot be disentangled in most of the experimentally interesting cases. Thus the many-body renormalization effects in such a coupled system are fundamentally nonmultiplicative in nature. Preliminary resutls of our findings have recently been reported.[8]

In order to make direct connections with experiments, we must take into account the finite thickness of the microstructures, namely the *quasi*-two-dimensional character of the electron wave functions and the rich variety of LO phonons (bulklike confined slab modes and interface slab modes) which are allowed in such thin-film geometries. Our third objective is to quantify the importance of the finite-thickness corrections on many-body effects. We find that they are substantive in weakening the electron-electron interaction and give rise to addition-

al structure in the quasiparticle damping rate in narrow quantum wells.

The motivation for this work is twofold. Intense, current experimental activity in GaAs-based 2D microstructures requires that detailed quantitative knowledge about quasiparticle properties be available. For example, quasiparticle effective mass is measured in cyclotron-resonance experiments, whereas quasiparticle damping can be measured in hot-electron spectroscopy. In spite of this great current interest in polar quasi-2D EG existing in GaAs quantum wells and heterostructures, there has been no detailed quantitative study of 2D quasiparticle properties including both electron-electron and electron-phonon interactions on an equal footing. One of our motivations for this work is to provide such a detailed quantitative study for this class of experimentally interesting systems.

A second more general motivation of our work, which is purely theoretical, is that we want to study a coupled electron-phonon many-body system treating electrons and phonons on an equal footing. Direct interaction between electrons via the Coulomb coupling and polar-electron–optical-phonon interaction (which is, of course, fundamentally Coulombic in origin, arising from the dynamical interaction between charge carriers and lattice ions) via Fröhlich coupling are perhaps the two most extensively studied many-body interactions in solid-state physics. Theorists have usually studied these two interactions in separate models without considering any mutual overlap between the interactions. Electron-electron Coulomb interaction has been traditionally studied in the context of electron-gas models neglecting phonons altogether, whereas Fröhlich interaction has been studied in the context of polaron models where only one electron interacts with the LO phonons. The electron-gas model has been helpful in understanding Coulomb interaction effects in metals, whereas the single-polaron model has been used in understanding carrier properties in ionic crystals and undoped semiconductors. The only important phonons for metals are acoustic phonons and, even though electron-phonon interaction in metals is a very extensively studied subject, the difference in energy scales between electrons (Fermi energy and plasma energy of approximately a few eV) and phonons (Debye energy of approximately a few meV) allows one to study the electron-electron and electron-phonon interactions totally separately. Screening of the electron-phonon interaction in metals can be quite correctly treated by the static screening approximation since electron energy scales are orders of magnitude larger than the phonon energies. Thus, in the context of metal physics a detailed study of the interplay between dynamical electron-electron and electron-phonon interactions is not relevant (which is perhaps the reason why such a calculation has never been carried out in the 3D EG). Similarly, in ionic crystals or in undoped compound semiconductors where Fröhlich electron–LO-phonon interaction is important, electron-electron interaction can be safely neglected because it is essentially a one-electron situation.

Intermediate between these two extremes (i.e., metals and ionic crystals) is the doped polar semiconductor situation. In these systems Fröhlich interactin is weak but non-negligible, and the presence of a finite density of free carriers makes Coulomb interaction significant as well. To the best of our knowledge, however, quasiparticle properties of such a *polar electron gas* have never been calculated treating electron-electron and electron-phonon interaction on an equal footing. At low electron density (when the plasmon has much lower energy than the LO phonon), screening is typically neglected, whereas at high electron density, the plasmon energy being much larger than the LO-phonon energy, one uses a statically screened Fröhlich interaction. The problem, of course, is that in doped semiconductors, electron-energy scales (Fermi and plasma energies) are comparable to the LO-phonon energy and the usual arguments made for metals simply do not apply. Clearly, a complete analysis based on treating electrons, phonons, and plasmons equivalently within the same approximation scheme is needed. We provide such an analysis based on the leading-order perturbation theory.

The diagrammatic theory used in our analysis is shown in Fig. 1. We obtain the electron self-energy from the effective dynamical electron-electron interaction. The effective interaction is obtained from the Coulomb electron-electron and the phonon-mediated electron-electron interaction in the bubble-diagram approximation ("the RPA"). The justification for calculating the electron self-energy in the leading order in the effective

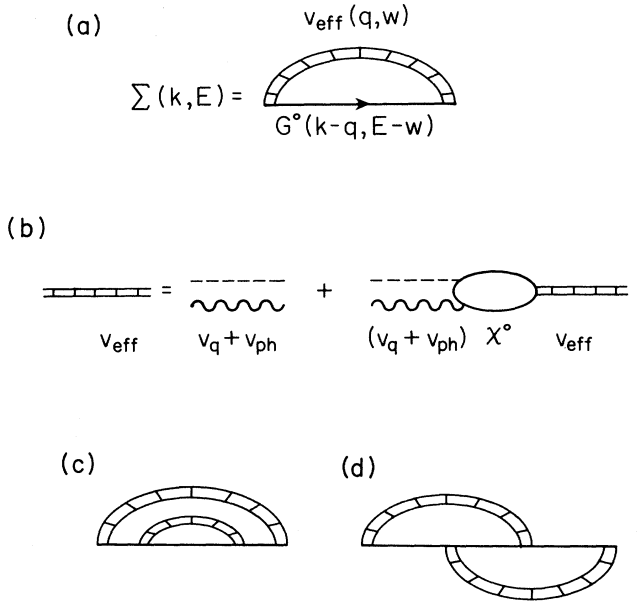

FIG. 1. (a) Electron self-energy in leading order in the effective dynamical interaction. (b) Effective dynamical interaction (hatched lines) V_{eff} calculated in the RPA. Dashed lines represent the Coulomb electron-electron interaction V_q, wiggly lines the LO-phonon-mediated electron-electron interaction V_{ph}, and the bubble the irreducible polarizability χ^0. Panels (c) and (d) show higher-order self-energy diagrams neglected in our calculation.

dynamical interaction is twofold: (1) In the "high-density" (low-r_s) limit, that is known to be a good approximation for the Coulomb interaction, whereas for weak Fröhlich coupling (valid for most polar III-V or II-VI *semiconductor* materials, but *not* for ionic crystals), usually the leading-order self-energy is adequate, and (2) the higher-order diagrams [such as (c) and (d) in Fig. 1] are simply intractable.

Our theory is strictly a zero-temperature theory, but we expect our results to be approximately valid at finite temperatures, provided the temperature is low enough such that $k_B T \ll E_F, \hbar\omega_{\rm LO}$ (where T, E_F, and $\omega_{\rm LO}$ are the temperature, the Fermi energy, and the LO-phonon frequency, respectively). At a typical low electron density of 2×10^{11} cm^{-2} in a GaAs system, the Fermi energy corresponds to a temperature of 80 K ($\approx E_F/k_B$), whereas $\hbar\omega_{\rm LO}/k_B \approx 427$ K for GaAs. Thus at low densities our results are quantitatively valid up to about 20 K, whereas at high densities ($\approx 10^{12}$ cm^{-2}), our results should be valid up to about 100 K.

This paper is organized as follows. In Sec. II we develop the formalism of the electron self-energy for the Coulomb interaction and for the Coulomb-plus-Fröhlich interaction in the two-dimensional case. We present and analyze results for the self-energy and spectral function, and we discuss the validity of the plasmon-pole approximation for two dimensions. In Sec. III we calculate the momentum distribution function and the renormalization factor for different densities. In Sec. IV we present the electronic density of states and discuss its experimental implications. In Sec. V we calculate various quasiparticle properties, namely the effective mass and the damping rate, discussing, in particular, the nonmultiplicative nature of the total renormalization, even in the weak-coupling limit, and the implications of the mode-coupling (also called plasmon-phonon coupling) phenomenon. In Sec. VI we study how the finite-thickness effects modify the results of the preceding sections. We provide a conclusion in Sec. VII. Throughout this article we refer to the situation having *both* Coulomb and Fröhlich interactions as the *coupled* system, whereas the situation with just the Coulomb interaction is called the *uncoupled* system.

II. ELECTRON SELF-ENERGY

Our model consists of a two-dimensional electron gas (2D EG) coupled to bulk dispersionless longitudinal-optical (LO) phonons at zero temperature. Electrons interact among themselves through the Coulomb interaction and through virtual-LO-phonon exchange via the Fröhlich interaction. The Coulomb potential in two-dimensional Fourier space is $V_q = 2\pi e^2/q\epsilon_\infty$, where ϵ_∞ is the optical (high-frequency) dielectric constant of the semiconductor. The LO-phonon-mediated electron-electron interaction is wave-vector and frequency dependent:

$$V_{\rm ph}(q,\omega) = M_q^2 D^0(\omega) \ . \tag{1}$$

M_q is the 2D Fröhlich matrix element[6] given by ($\hbar=1$ throughout this paper)

$$M_q^2 = V_q \frac{\omega_{\rm LO}}{2}\left[1-\frac{\epsilon_\infty}{\epsilon_0}\right] \equiv \frac{2\pi\alpha(\omega_{\rm LO})^{3/2}}{q(2m)^{1/2}} \ , \tag{2}$$

where $\omega_{\rm LO}$ is the LO-phonon frequency, ϵ_0 is the static dielectric constant of the semiconductor, $\alpha = e^2\sqrt{m/2\omega_{\rm LO}}(1/\epsilon_\infty - 1/\epsilon_0)$ is the so-called Fröhlich coupling constant, which is a dimensionless measure of polar coupling in the material, m is the bulk (band-structure) effective mass, and

$$D^0(\omega) = \frac{2\omega_{\rm LO}}{\omega^2-\omega_{\rm LO}^2+i\gamma} \tag{3}$$

is the unperturbed LO-phonon propagator ($\gamma = 0^+$ throughout this paper). More details about our basic model can be found in the literature (cf. Das Sarma and Mason in Ref. 6) and are not given here.

The effective electron-electron interaction is obtained in the RPA (Ref. 9) [Fig. 1(b)] by summing *all* the bubble diagrams:

$$V_{\rm eff}(q,\omega) = \frac{V_q + V_{\rm ph}(q,\omega)}{1-[V_q+V_{\rm ph}(q,\omega)]\chi^0(q,\omega)} = \frac{V_q}{\epsilon_t(q,\omega)} \ , \tag{4}$$

where χ_0 is the time-ordered irreducible polarizability of the 2D EG. For $\omega > 0$ the noninteracting polarizability (the "bare bubble") can be easily calculated[10] to be

$$\chi^0(q,\omega) = -\frac{N}{E_F}\frac{k_F}{q}\left[\frac{q}{k_F} - (a_+^2-1)^{1/2} + (a_-^2-1)^{1/2}\right] , \tag{5}$$

where N is the 2D electron density, $a_\pm = (\omega+i\gamma)/qv_F \pm q/2k_F$, and the complex square roots are to be chosen to be the branch with positive imaginary part. Subscript F corresponds to quantities at the Fermi energy (i.e., E_F, k_F, and v_F are the Fermi energy, the Fermi wave vector, and the Fermi velocity, respectively). For $\omega < 0$ we have $\chi^0(q,\omega) = \chi^0(q,-\omega)$. $\epsilon_t(q,\omega)$ is the total dielectric function, which has an electron and a phonon component:

$$\epsilon_t(q,\omega) = 1 - V_q\chi^0(q,\omega) + \frac{1-\epsilon_\infty/\epsilon_0}{\epsilon_\infty/\epsilon_0 - \omega^2/\omega_{\rm LO}^2} \ . \tag{6}$$

The electron self-energy of the coupled system can be expanded in the effective interaction $V_{\rm eff}$, and, neglecting vertex corrections it is given by

$$\Sigma_t(k,E) = \frac{i}{(2\pi)^3}\int d^2q \int d\omega \, V_{\rm eff}(q,\omega) G^0(\mathbf{k}-\mathbf{q}, E-\omega) \ , \tag{7}$$

where G^0 is the Green function for the noninteracting electron gas,

$$G^0(k,E) = \frac{1}{E-\xi(k)+i\gamma\,{\rm sgn}(k-k_F)} \ , \tag{8}$$

with $\xi(k) = (k^2-k_F^2)/2m$. Equation (7) [Fig. 1(a)] is the

basic starting point of this work.

$V_{\rm eff}$ given by Eq. (4) can be written[9] as

$$V_{\rm eff}(q,\omega)=\frac{V_q}{\epsilon(q,\omega)}+\frac{M_q^2}{\epsilon^2(q,\omega)}D(q,\omega)\ , \tag{9}$$

where $\epsilon(q,\omega)=1-V_q\chi^0(q,\omega)$ is the purely electronic dielectric function and

$$D(q,\omega)=\frac{2\omega_{\rm LO}}{\omega^2-\omega_{\rm LO}^2-2\omega_{\rm LO}M_q^2\chi^0(q,\omega)/\epsilon(q,\omega)} \tag{10}$$

is the *renormalized* phonon propagator. The decomposed expression of Eq. (9) indicates that the electron self-energy $\Sigma_t(k,E)$ of the coupled 2D EG can be written as

$$\Sigma_t(k,E)=\Sigma(k,E)+\Sigma_{\rm ph}(k,E)\ , \tag{11}$$

where

$$\Sigma(k,E)=\frac{i}{(2\pi)^3}\int d^2q\int d\omega[V_q/\epsilon(q,\omega)]G_0(\mathbf{k}-\mathbf{q},E-\omega)\ ,$$

and

$$\Sigma_{\rm ph}(k,E)=\frac{i}{(2\pi)^3}\int d^2q\int d\omega[M_q^2D(q,\omega)/\epsilon^2(q,\omega)]\times G_0(\mathbf{k}-\mathbf{q},E-\omega)\ .$$

The first term is the Coulomb (or electronic) contribution to the electron self-energy and represents the self-energy obtained when the electron gas is not coupled to phonons (uncoupled 2D EG). As with the dielectric function, we reserve quantities without subscript for purely the electronic contribution (i.e., when Fröhlich interaction is absent). The second term is called the phonon contribution to the electron self-energy. This name is, however, misleading, because $\Sigma_{\rm ph}$ has contributions from electronic screening and is not a well-defined self-energy since it does not fulfill the usual analyticity requirements (i.e., its imaginary part is not always negative above the Fermi energy). The expression for $\Sigma_{\rm ph}$ has been used as a starting point for making simple approximations, for example, by setting $\epsilon(q,\omega)=\epsilon(q,0)$ one gets the static screening approximation, and by setting $\epsilon(q,\omega)=1$ one gets the unscreened approximation. The calculation of dynamical $\Sigma_{\rm ph}$ is not convenient from the numerical point of view because the singularities of $1/\epsilon^2$ are much more complex to treat than the singularities of $1/\epsilon_t$. Therefore, we calculate Σ and Σ_t; $\Sigma_{\rm ph}$ can be obtained from their difference. We emphasize that $\Sigma_{\rm ph}$ by itself is *not* a physically relevant (or mathematically well-defined) quantity in the dynamical situation since it might give rise to "negative damping rate."[6] Σ depends only on the dimensionless interparticle separation parameter $r_s=(a_B^*\sqrt{\pi N})^{-1}$, $a_B^*=\epsilon_\infty/e^2m$ being the effective Bohr radius. On the other hand, Σ_t depends on the electron density (or r_s), the phonon and electron energy scales (through $\omega_{\rm LO}$ and E_F), and the electron-phonon–coupling strength (through ϵ_0 and ϵ_∞).

For most of our numerical calculations we use the parameters corresponding to GaAs: $m=0.07m_e$ (m_e is the free-electron mass), $\epsilon_0=12.9$, $\epsilon_\infty=10.9$, and $\omega_{\rm LO}=36.8$ meV. We emphasize that GaAs is a weakly coupled electron-phonon system ($\alpha=0.07$ for GaAs). Our results for Σ are generally valid for the uncoupled 2D EG, while our results for Σ_t are representative of the weakly coupled 2D EG–phonon system. From now on we will measure wave vectors in units of $2k_F$ and energies and self-energies in units of $4E_F$ [i.e., $\xi(k)=k^2-0.25$].

In order to calculate Σ, we first separate out the Hartree-Fock or the exchange contribution:

$$\Sigma^{\rm HF}(k)=\begin{cases}-\rho\left[(0.5-k)\pi+\displaystyle\int_{0.5-k}^{0.5+k}dq\ \arccos\left[\frac{k^2+\xi(q)}{2kq}\right]\right], & 0<k<0.5 \quad (12a)\\ -\rho\displaystyle\int_{k-0.5}^{k+0.5}dq\ \arccos\left[\frac{k^2+\xi(q)}{2kq}\right], & k>0.5 \quad (12b)\end{cases}$$

$$\rho=r_s/\sqrt{2}\pi\ .$$

For the remaining part we perform the standard[11,2] contour deformation in the complex ω plane and obtain a line and a pole contribution:

$$\Sigma(k,E)=\Sigma^{\rm HF}(k)+\Sigma^L(k,E)+\Sigma^P(k,E)\ , \tag{13}$$

$$\Sigma^L(k,E)=\rho\int_0^\infty dq\int_0^\infty dq\int_0^\infty dy\left[\frac{1}{\epsilon(q,iy)}-1\right]{\rm Re}\left[\frac{1}{\{[k^2+\xi(q)-E+iy]^2-(2kq)^2\}^{1/2}}\right]\ , \tag{14a}$$

$$\Sigma^P(k,E)=\rho\int_0^\infty dq\int_{k^2+\xi(q)-2kq}^{k^2+\xi(q)+2kq}dy\left[\frac{1}{\epsilon(q,E-y)}-1\right]\frac{\Theta(E-y)-\Theta(-y)}{\{(2kq)^2-[k^2+\xi(q)-y]^2\}^{1/2}}\ . \tag{14b}$$

The complex square roots are taken on the branch with positive imaginary part throughout this paper. $\Theta(x)$ is the Heaviside step function. For $k=0$ the angular integrations are easily done, with the result

$$\Sigma^{\rm HF}(k=0)=-\rho\pi/2\ , \tag{15a}$$

$$\Sigma^L(k=0,E)=\rho\int_0^\infty dq\int_0^\infty dy\left[\frac{1}{\epsilon(q,iy)}-1\right]\times\frac{\xi(q)-E}{[\xi(q)-E]^2+y^2}\ , \tag{15b}$$

$$\Sigma^P(k=0,E)=\rho\pi\int_{0.5}^{s(E)}dq\left[\frac{1}{\epsilon(q,E-\xi(q))}-1\right], \quad (15c)$$

where $s(E)=\Theta(0.25+E)\sqrt{0.25+E}$. The self-energy Σ_t of the coupled 2D EG is obtained by replacing ϵ by ϵ_t in (14) and (15). The integrals were numerically evaluated using adaptive and open Simpson integration.[12] The singularities of ϵ were treated by the replacement $-V_q\chi^0\rightarrow -V_q\chi^0+i\delta$ with $\delta=0.001$. The insensitivity of the final results to the specific value of δ was checked. A further check was not to rely on the broadening parameter δ, but to use the correct particle-conserving form of the electron polarizability suggested by Mermin:[13]

$$\chi_c^0(q,\omega)=\frac{(1+i/\omega\tau)\chi^0(q,\omega+i/\tau)}{1+(i/\omega\tau)\chi^0(q,\omega+i/\tau)/\chi^0(q,0)}, \quad (16)$$

with χ^0 given by (5) and the impurity-scattering time τ related to the mobility μ by $1/\tau=e/m\mu$. We chose $\mu=5\times10^4$ cm^2/V s (which is *not* a particularly high value by the standards of GaAs technology), so that $1/\tau\simeq0.3$ meV. Making this correction or changing $1/\tau$ by small amounts did not lead to significant changes in Σ or Σ_t.

Quasiparticle excitation energies of the system are obtained from the self-energy Σ by solving Dyson's equation:

$$E+\mu=\xi(k)+\mathrm{Re}\Sigma(k,E), \quad (17)$$

where E is measured relative to the chemical potential μ, which is determined by setting $E=0$ and $k=0.5$ in the above equation.[2]

The single-particle spectral function is given by

$$A(k,E)=\frac{1}{\pi}\frac{\mathrm{Im}\Sigma(k,E)\mathrm{sgn}(-E)}{[E+\mu-\xi(k)-\mathrm{Re}\Sigma(k,E)]^2+[\mathrm{Im}\Sigma(k,E)]^2}. \quad (18)$$

Its peaks correspond to the nearly undamped solutions of Dyson's equation. The spectral function is a probability density and verifies the sum rule

$$\int_{-\infty}^{+\infty}dE\ A(k,E)=1. \quad (19)$$

In all our calculations, the sum rule (19) is fulfilled within one percent. The same error may be taken as a measure of the numerical accuracy of our results.

Figure 2 shows the typical behavior of the self-energy and spectral function for uncoupled (thin lines) and coupled (thick lines) systems in a low-density sample ($N=2\times10^{11}$ cm^{-2}, $r_s=1.5$). The intersections of ReΣ and the straight lines $E+\mu-\xi(k)$ indicate the solutions to Dyson's equation. For the uncoupled 2D EG and the lowest wave vector ($k=0.1$) there are three solutions. If we enumerate them according to increasing distance from $E=0$, the first is the regular quasiparticle solution (i.e., a bare particle surrounded by a cloud of virtual plasmons and particle-hole excitations) which is slightly shifted from the noninteracting value $E=\xi(k)$. Since the imaginary part is much smaller than the real part, the quasiparticle is a well-defined excitation of the system and shows up as a sharp peak in the spectral function. The second solution is damped and gives no contribution to A. The third solution is only weakly damped and produces a second peak in the spectral function. This solution which is well studied in three dimensions, has been called a plasmaron and is interpreted as a hole coupled to a cloud of real plasmons.[2] In three dimensions it has been shown[2] that the plasmaron remains a well-defined excitation of the system even after a second iteration of Dyson's equation. The oscillator strength of the plasmaron for the conditions of Fig. 2 is significant when compared to that of the quasiparticle excitation (0.14 versus 0.42). For very small wave vectors the plasmaron becomes undamped, giving rise to a δ function in A. For wave vectors $k\gtrsim0.15$ we no longer have three solutions to Dyson's equation, as the straight line falls below the minimum of ReΣ. The plasmaron is then a long-wavelength excitation. For the Fermi wave vector

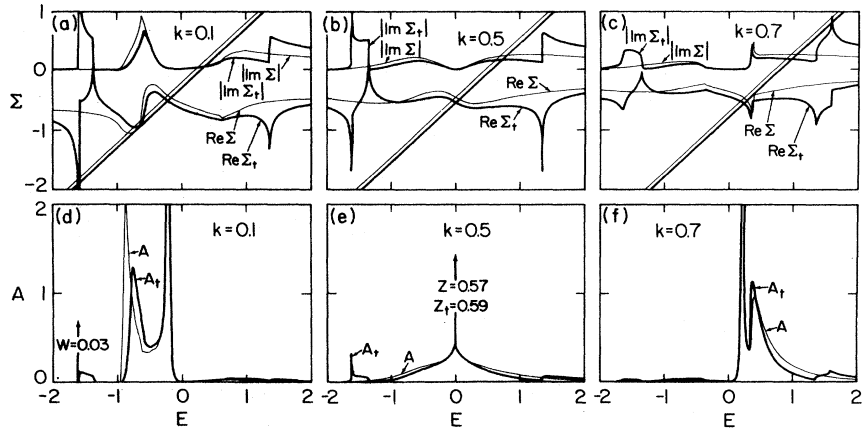

FIG. 2. (a)–(c) Self-energy $\Sigma(k,E)$ and (d)–(e) spectral function $A(k,E)$ as functions of the energy E for three fixed wave vectors $k=0.1$, 0.5, and 0.7. Thin (thick) lines correspond to the uncoupled (coupled) 2D EG. The electron density is $N=2\times10^{11}$ cm^{-2}. Wave vectors are measured in units of $2k_F=2.2\times10^{16}$ cm^{-1}, energies and self-energies in units of $4E_F=27.4$ meV, and spectral functions in units of $(4E_F)^{-1}$. The LO-phonon energy is $\omega_{LO}=1.35$. The straight lines are given by $E+\mu-\xi(k)$, and their intersections with ReΣ indicate the solutions to Dyson's equation. $|\mathrm{Im}\Sigma|$ is plotted instead of ImΣ for clarity of the drawings. [Im$\Sigma=\mp|\mathrm{Im}\Sigma|$ for $E>0$ ($E<0$).]

($k=0.5$) there is only one solution to Dyson's equation and a strong peak (δ function) in A since the quasiparticle at the Fermi surface is undamped. The oscillator strength of the quasiparticle is called the renormalization factor Z. In Sec. III we give details of its calculation. Its value is considerably smaller than unity, indicating that the satellites of the quasiparticle have significant oscillator strength. For $k=0.7$ there is also only one solution to Dyson's equation, the regular quasiparticle solution.

In the 3D EG (Refs. 2 and 14) the finite frequency of the long-wavelength plasmon ω_p produces a logarithmic singularity in $\mathrm{Im}\Sigma$ and a finite discontinuity in $\mathrm{Re}\Sigma$ at $E=\xi(k)\pm\omega_p$ for $k>0.5$ ($k<0.5$). In the 2D EG the long-wavelength plasmon frequency vanishes and the above structure is not present. However, there are weaker singularities where $\mathrm{Im}\Sigma$ has a sharp peak and $\mathrm{Re}\Sigma$ an abrupt step. The locations of these singularities are not associated with characteristic frequencies, but are approximately given by the solution to the following cubic equation,

$$u^3-k^2u^2\mp 0.4r_sku\pm 0.35r_sk^3+0.01r_s^2=0\ , \qquad (20)$$

in the interval $k^2<u<4/3k^2$ ($k^2>u$) for $k>0.5$ ($k<0.5$), with $u=E+0.25$. In obtaining Eq. (20) we have imposed the phase-space restrictions for plasmon emission and used the long-wavelength form of the plasmon dispersion. The location of the singularity is then accurately given by (20) only when a very small momentum transfer is involved $[|k-(4k^2-3u)^{1/2}|/3\ll 1]$, which is satisfied for $k\gtrsim 0.4$. It can be seen from Fig. 2 that, for $k=0.7$, Eq. (20) gives a good account of the singularity, while for $k=0.1$ it does not.

For the low-density sample of Fig. 2 ($N=2\times10^{11}$ cm^{-2}) the phonon energy is much larger than the Fermi energy ($\omega_{\mathrm{LO}}=1.35$, in units of $4E_F$) and the phonon structure is almost decoupled from the electron structure. The electron structure ($|E|\lesssim 1$) of Σ_t is similar to that of Σ, the main difference being a rigid shift of the real part towards more negative values. The phonon structure is confined to $|E|\gtrsim\omega_{\mathrm{LO}}$ and has the same behavior as that of a polaron (a *single* electron coupled to phonons).[6] For long wavelengths, $1/\epsilon_t(q,\omega)$ is singular at ω_{LO}, causing a logarithmic singularity in $\mathrm{Im}\Sigma_t$ and a finite discontinuity in $\mathrm{Re}\Sigma_t$ at $E=\xi(k)\pm\omega_{\mathrm{LO}}$ for $k>0.5$ ($k<0.5$). This is similar to the structure found in the uncoupled 3D EG case due to the finite frequency of the long-wavelength plasmon. $\mathrm{Re}\Sigma_t$ has weak logarithmic singularities and $\mathrm{Im}\Sigma_t$ has finite discontinuities at $E=\pm\omega_{\mathrm{LO}}$. This singularity appears whenever the system has a dispersionless mode.[2] For this low electron density the mode coupling[7] between phonons and plasmons is very small (see Sec. V) and the phononlike mode remains close to ω_{LO} for all wave vectors q. For the lowest wave vector ($k=0.1$) shown in Fig. 2, A_t has three peaks. Starting from $E=0$, the first is the quasiparticle, at almost the same energy as that of the uncoupled 2D EG. The second peak represents the plasmaron, which is more damped and closer to the Fermi energy than the plasmaron of the uncoupled 2D EG. The third peak is a δ function and corresponds to an undamped solution of Dyson's equation around $E=-\omega_{\mathrm{LO}}-0.25$ analogous to the plasmaron. Its oscillator strength, indicated by W in Fig. 2, is very small. However, its signature appears in the density of states, as we discuss in Sec. IV. For the Fermi wave vector ($k=0.5$), A_t has two peaks: the undamped quasiparticle at $E=0$, and a sharp peak around $E=-\omega_{\mathrm{LO}}-0.25$. The coupling to phonons is reflected in a slightly increased renormalization factor ($Z_t=0.59$), a smaller oscillator strength of the quasiparticle satellite for $0<|E|<\omega_{\mathrm{LO}}$, and the new structure for $|E|\gtrsim\omega_{\mathrm{LO}}$. For $k=0.7$ the singularity associated with the plasmon emission is slightly shifted towards the Fermi energy since *the phonon screening reduces the plasmon frequency.* $\mathrm{Re}\Sigma_t$ diverges at $E=\pm\omega_{\mathrm{LO}}$ and $\mathrm{Im}\Sigma_t$ diverges at $E=\xi(k)+\omega_{\mathrm{LO}}$.

For a given wave vector, with increasing electron density the main change in the uncoupled self-energy is in its scale (decreasing with r_s), but its general behavior remains unaltered (Fig. 3). Small changes in the self-energy may, however, have important effects on the spectral function if they occur near the solutions of Dyson's equation. For example, change in the electron density can result in a loss of the plasmaron solution.

The self-energy of the coupled system is strongly dependent on the electron density. As the electron density is increased, the LO-phonon energy becomes comparable to the Fermi energy and the phonon structure moves towards lower energies, mixing with the electron structure. With increasing N the mode coupling becomes stronger (see Sec. V) and the singularities at $E=\pm\omega_{\mathrm{LO}}$ weaker because the coupled plasmon-phonon modes are not dispersionless. This behavior is illustrated in Fig. 3, where Σ and A are shown for two electron densities at a given wave vector.

We conclude this section by discussing the plasmon-

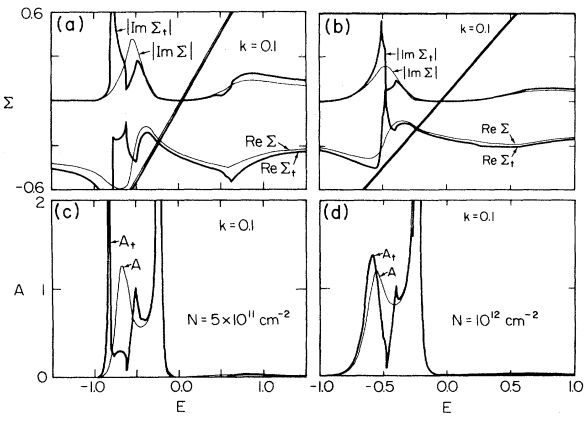

FIG. 3. (a),(b) Self-energy $\Sigma(k,E)$ and (c),(d) spectral function $A(k,E)$ as functions of the energy E for $k=0.1$ and electron densities $N=5\times10^{11}$ cm^{-2} [(a) and (c)] and $N=10^{12}$ cm^{-2} [(b) and (d)]. Thin (thick) lines correspond to the uncoupled (coupled) 2D EG. The units are the same as in Fig. 2, but for $N=5\times10^{11}$ cm^{-2}, $2k_F=3.5\times10^6$ cm^{-1} and $4E_F=68.5$ meV, while for $N=10^{12}$ cm^{-2}, $2k_F=5.0\times10^{-6}$ cm^{-1} and $4E_F=137$ meV.

pole approximation. The single-plasmon-pole approximation (SPP) has been extensively used both in the 3D EG (Refs. 2 and 15) and the 2D EG.[16,17] Its use in the three-dimensional case has been justified by detailed calculations of Lundqvist,[2] where the SPP and RPA results were compared. We do not know of an equivalent justification in the 2D EG; consequently, in Fig. 4 we compare SPP and RPA results for the electron self-energy and the spectral function. The real part of the self-energy is obtained, after doing a one-dimensional integral, using the formulas derived by Vinter.[16] The imaginary part is straightforward and can also be obtained as a one-dimensional integral. The chemical potential and the spectral function are given by (17) and (18), respectively. From Fig. 4 it is clear that the agreement between the RPA and SPP approximation is much poorer in the 2D EG than in the 3D EG case.[2] In particular, the singularity around $E=-1.0$ is an artifact of the softness of the plasmon dispersion in the 2D EG and gives rise to two spurious solutions of Dyson's equation (one undamped and the other damped). The SPP approximation then overestimates the plasmaron, giving it spectral weight for wave vectors at which it does not exist. The plasmon-pole quasiparticle solution is displaced with respect to the RPA solution (except for $k=0.5$) and is completely undamped. The spectral weight of the various δ functions cannot be directly extracted from the plasmon-pole results. We have recently provided[18] an experimentally testable failure of the SPP approximation in the context of band-gap renormalization of two-dimensional semiconductor systems.

The use of the RPA itself is less justified in two than in three dimension,[19] since the interactions effects (as we can see from this work) are more important as we go to lower dimensionality. Theoretical efforts have recently been made to go beyond the RPA by incorporating local-field corrections in a consistent and tractable fashion.[17] However, these calculations were performed within the framework of the SPP approximation and, thus, the numerical results cannot be trusted. Any improvement of the RPA should start from the RPA itself and not from poor approximations to it. For the electron-phonon interaction the SPP approximation runs into the difficulty that it cannot include Landau damping for large-wave-vector plasmons.

III. MOMENTUM DISTRIBUTION AND RENORMALIZATION FACTOR

The momentum distribution

$$n(k)=\int_{-\infty}^{0} dE\, A(k,E) \tag{21}$$

is shown in Fig. 5 for the uncoupled (n) and coupled (n_t) systems for various electron densities. These curves exhibit the expected features, with states above the Fermi surface ($k>0.5$) occupied and states below the Fermi surface ($k<0.5$) unoccupied. The departure from the noninteracting case becomes stronger as the density is decreased. Comparing the momentum distribution n of the uncoupled 2D EG to the three-dimensional results of Lundqvist,[2] we see that for an equivalent r_s the distribution function in the 3D EG is closer to the noninteracting momentum distribution, indicating that many-body effects are more significant in two dimensions than in three.

For a given electron density n_t is very close to n, indicating that the inclusion of the electron-phonon coupling has a very small effect on the momentum distribution for weak electron-phonon coupling. However, this small change is not uniform over all wave vectors. For low densities ($N=10^{11}$ cm^{-2}), n and n_t are almost equal, except in the neighborhood of the Fermi surface, where n_t

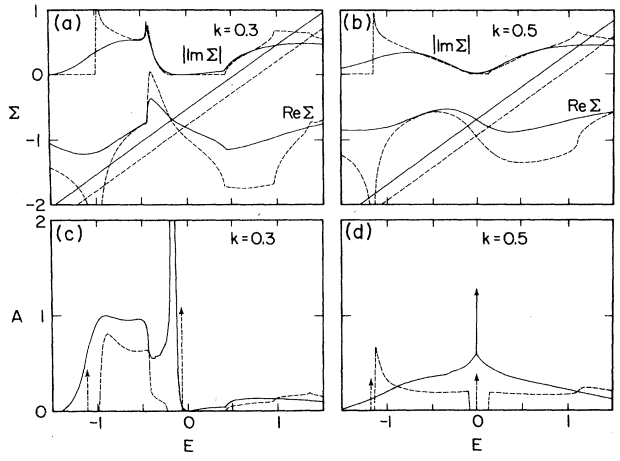

FIG. 4. (a),(b) Self-energy $\Sigma(k,E)$ and (c),(d) spectral function $A(k,E)$ as functions of the energy E for two fixed wave vectors $k=0.3$ and 0.5. Solid lines correspond to the RPA results and dashed lines to the plasmon-pole results. The units are the same as in Fig. 2. The electron density is $N=10^{11}$ cm^{-2} and $4E_F=13.7$ meV. The arrows represent δ functions, and their heights do not indicate the spectral weights.

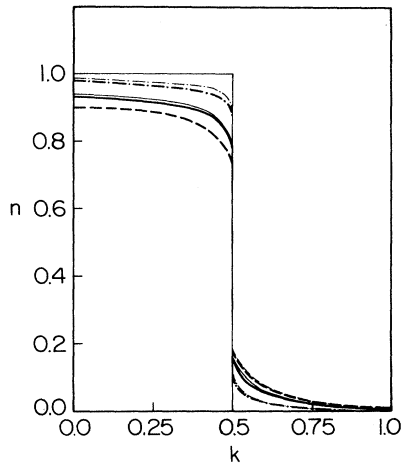

FIG. 5. Momentum distribution for the uncoupled (thin lines) and coupled (thick lines) 2D EG. Dashed lines correspond to $N=10^{11}$ cm^{-2}, solid lines $N=2\times10^{11}$ cm^{-2}, and dashed-dotted lines $N=10^{12}$ cm^{-2}. The step function of the noninteracting momentum distribution is indicated by a thin solid line. Wave vectors are measured in units of $2k_F$.

is slightly closer to the noninteracting case, showing a sharper discontinuity at the Fermi surface. For the other two densities of Fig. 5, n is closer than n_t to the noninteracting distribution, except in the neighborhood of the Fermi surface, where their behavior is interchanged.

The size of the discontinuity at the Fermi surface is given by the renormalization factor Z. It can be easily seen[9,2] that Z corresponds to the oscillator strength of the undamped quasiparticle at the Fermi surface and can be calculated as

$$Z=\left[1-\frac{\partial\Sigma}{\partial E}\right]^{-1}\Bigg|_{k=0.5,\ E=0}=(1-I^L-I^P)^{-1}\ . \tag{22}$$

As with the self-energy, we write the partial derivative as the sum of a line and a pole contribution,

$$I^L=\rho\int_0^\infty dq\int_0^\infty dy\frac{1}{\epsilon(q,iy)}\mathrm{Re}\left[\frac{q^2+iy}{[(q^2+iy)^2-q^2][(q^2+iy)^2-q^2]^{1/2}}\right], \tag{23}$$

$$I^P=\rho\int_0^1 dq\frac{1}{\epsilon(q,0)}\frac{1}{q(1-q^2)^{1/2}}=\begin{cases}\dfrac{2\beta}{\pi\zeta}\left[\arctan\left[\dfrac{\beta+1}{\zeta}\right]-\arctan\left[\dfrac{1}{\zeta}\right]\right] & \text{for } \beta>1, \quad (24a)\\[2ex] \dfrac{\beta}{\pi\zeta}\ln\left[\dfrac{\beta+1-\zeta}{\beta+1+\zeta}\dfrac{1+\zeta}{1-\zeta}\right] & \text{for } \beta<1, \quad (24b)\end{cases}$$

where $\beta=r_s/\sqrt{2}$ for the uncoupled 2D EG and $\beta=(r_s/\sqrt{2})(\epsilon_0/\epsilon_\infty)$ for the coupled 2D EG, $\zeta=|1-\beta^2|^{1/2}$. The renormalization factor can also be calculated by taking numerical derivatives in Eq. (14). Both methods yield the same Z with 0.5%, giving another estimate of the numerical accuracy of our results. In Table I we give Z and Z_t for different electron densities. These values are consistent with the graphs of Fig. 5. For the interval of densities considered, Z_t is always greater than Z and the difference increases as we go to lower N.

IV. DENSITY OF STATES

The density of states (DOS) is given by

$$g(E)=2\int\frac{d^2k}{(2\pi)^2}A(k,E)\ . \tag{25}$$

For a noninteracting 2D EG we have

$$g_{\mathrm{ni}}(E)=\begin{cases}0 \text{ if } E<-0.25\ , & (26a)\\ m/\pi=g^0 \text{ if } E>-0.25\ . & (26b)\end{cases}$$

Figure 6 gives the DOS for the uncoupled (g) and coupled (g_t) systems, together with the DOS of the noninteracting 2D EG (g_{ni}). In all cases the DOS is normalized with respect to g^0. The shaded area represents the occupied states of the noninteracting 2D EG and is equal (within 2%) to the area below $E=0$ for each of the interacting cases. For the uncoupled 2D EG and the lowest density considered ($N=10^{11}$ cm^{-2}), there is an important departure from the noninteracting case. A long tail develops and, consequently, the DOS at the Fermi energy is considerably reduced (by about 42%) from its noninteracting value. The peak around $E=-1.0$ is associated with the plasmaron. Since the plasmaron is undamped in a narrow energy region, the peak is very sharp. For $N=2\times10^{11}$ cm^{-2} the results are similar, but the tail is not as long, $g(0)\simeq0.65$, and the plasmaron

TABLE I. Calculated values of the renormalization factors Z and Z_t.

$N(10^{11}$ cm$^{-2})$	r_s	Z	Z_t
1	2.2	0.503	0.522
2	1.5	0.574	0.591
4	1.1	0.646	0.657
7	0.8	0.701	0.707
10	0.7	0.734	0.737

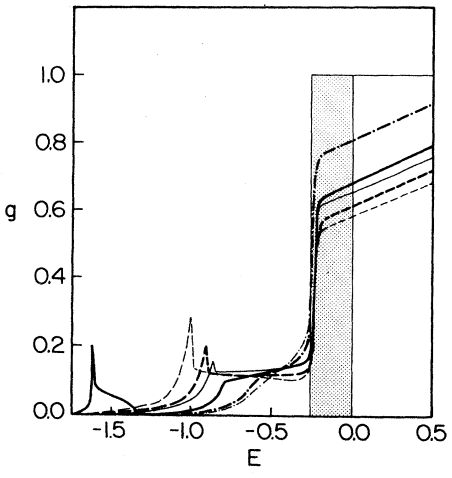

FIG. 6. Density of states for the uncoupled (thin lines) and coupled (thick lines) 2D EG. Dashed lines correspond to $N=10^{11}$ cm^{-2}, solid lines $N=2\times10^{11}$ cm^{-2}, and dashed-dotted lines $N=10^{12}$ cm^{-2}. The step function of the noninteracting DOS is indicated by a thin solid line. The shaded area represents the occupied states in the noninteracting 2D EG. Energies are measured in units of $4E_F$ and densities of states are measured in units of the noninteracting value $g^0=2.9\times10^{13}$ cm^{-2} eV^{-1}. In our units, the LO-phonon energy for the above densities is 2.69, 1.35, and 0.27, respectively.

peak is smaller and closer to the Fermi energy. For the highest density considered ($N=10^{12}$ cm^{-2}) the situation is closest to the noninteracting case, $g(0)\simeq 0.80$, and there is no observable plasmaron peak in the low-energy tail.

When the electron-phonon interaction is turned on, the change from g to g_t is strongly dependent on the electron density. For $N=10^{11}$ cm^{-2} the phonon structure is far from the Fermi energy ($|E|\gtrsim\omega_{\rm LO}=2.69$) and is not visible in Fig. 6. At low densities the LO-phonon frequency is much larger than the characteristic electronic frequencies and *the electron-phonon interaction is effective in screening the electron-electron interaction.* This is reflected in a smaller low-energy tail, an enhancement of the DOS at the Fermi energy [$g_t(0)\simeq 0.61$], and the shifting of the plasmaron peak towards the Fermi energy. For $N=2\times 10^{11}$ cm^{-2} the phonon structure is visible in the interval $-\omega_{\rm LO}-0.25\le E\le\omega_{\rm LO}$ and its sharp peak is associated with the new solution of Dyson's equation in the coupled 2D EG. The plasmaron is more damped than in the uncoupled 2D EG and no longer gives a peak in the DOS, but, instead, a cusp. The DOS at the Fermi energy is slightly enhanced with respect to the uncoupled case [$g_t(0)\simeq 0.68$]. For $N=10^{12}$ cm^{-2}, g and g_t are very similar, indicating that at high densities the Coulomb interaction screens the electron-phonon interaction.

To the best of our knowledge, a direct observation of the plasmaron in the 3D EG has not yet been achieved. However, in the 2D EG the plasmaron peak of the DOS is considerably sharper than the corresponding three-dimensional one and its observation in tunneling or photoemission experiments is expected to be easier.

V. EFFECTIVE MASS AND DAMPING RATE

The effective mass is defined by

$$m^*=k\left[\frac{dE(k)}{dk}\right]^{-1}\Bigg|_{k=0.5}. \tag{27}$$

In leading-order perturbation theory[20] the quasiparticle energy is given by

$$E(k)=\xi(k)+\mathrm{Re}\Sigma(k,\xi(k))\ , \tag{28}$$

and, then,

$$\frac{m^*}{m}=\left[1+\frac{\partial\Sigma}{\partial E}+\frac{m}{k}\frac{\partial\Sigma}{\partial k}\right]^{-1}\Bigg|_{k=0.5,\ E=0}$$
$$=(1+I^L+I^P)^{-1}\ . \tag{29}$$

The momentum derivative does not give a pole contribution, so that I^P is still given by (24). The line contribution is

$$I^L=\rho\int_0^\infty dq\int_0^\infty dy\frac{1}{\epsilon(q,iy)}\mathrm{Re}\left[\frac{2q^2}{[(q^2+iy)^2-q^2][(q^2+iy)^2-q^2]^{1/2}}\right]. \tag{30}$$

The effective mass for interacting electrons in the surface inversion layer of silicon has been calculated by Vinter[16] using the plasmon-pole approximation and a different definition than (29), and by Ting, Lee, and Quinn[21] using the RPA and Eq. (29). The RPA results are in good agreement with the experimental values, and this agreement becomes even better after the assumptions of the ideal 2D EG are relaxed by including finite thickness, multisubband occupation, etc. in the theory.

Figure 7 gives m^*/m for uncoupled (thin lines) and coupled (thick lines) systems as a function of the interparticle separation parameter r_s. The behavior for the uncoupled 2D EG is similar to that of the 3D EG.[18] However, for equivalent r_s the 2D EG has a larger mass correction ($|m^*-m|/m$) than the 3D EG, indicating again that the many-body effects are more important in two than in three dimensions. The inclusion of the electron-phonon coupling causes a small departure from the previous case, reducing the mass correction for low ($r_s>1.4$) and high ($r_s<0.7$) densities and enhancing the mass correction at intermediate densities. The small departure of the coupled results from the uncoupled ones is an effect of the weak-electron-phonon coupling in GaAs. The departure becomes increasingly more impor-

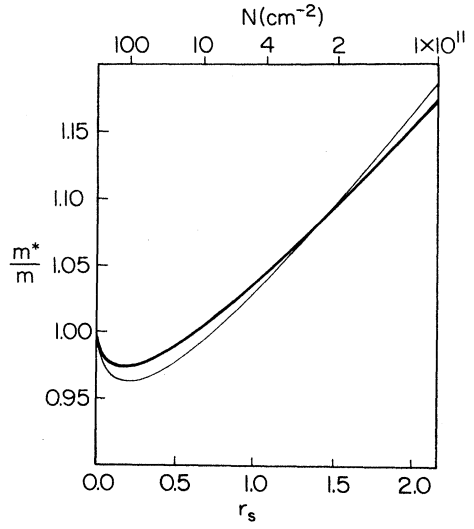

FIG. 7. Effective mass for the uncoupled (thin lines) and coupled (thick lines) 2D EG as a function of the dimensionless interparticle separation parameter r_s. On the upper horizontal scale some values of the electron density N are indicated. (The relationship between r_s and N is given in the text.)

tant as we go to higher couplings, as we discuss in Sec. VII.

The damping rate is given by the imaginary part of the quasiparticle self-energy $\Gamma(k)=|\mathrm{Im}\Sigma(k,\xi(k))|$. The quasiparticle lifetime $[2\Gamma(k)]^{-1}$ and the inelastic mean free path $l_k=k/2m\Gamma(k)$ are of special experimental interest. Figure 8 gives $\Gamma(k)$ for uncoupled and coupled 2D EG's as a function of k for low and high electron densities. At the Fermi surface the quasiparticle is always undamped and $\Gamma(0.5)=0$. For the uncoupled 2D EG there are two kinds of processes that may cause scattering of the quasiparticle: excitation of electron-hole pairs and excitation of plasmons. The former is the dominant scattering mechanism for low k; the latter turns on at a threshold wave vector k_c, giving rise to a sharp increase of $\Gamma(k)$, with $k_c=q_c+0.5$ (q_c being the minimum momentum transfer, where the plasmon dispersion curve enters the electron-hole continuum). The main difference between the low- and high-density cases for the uncoupled 2D EG appears in the scale of the damping rate when expressed in units of $4E_F$ (in absolute units, however, this difference is small).

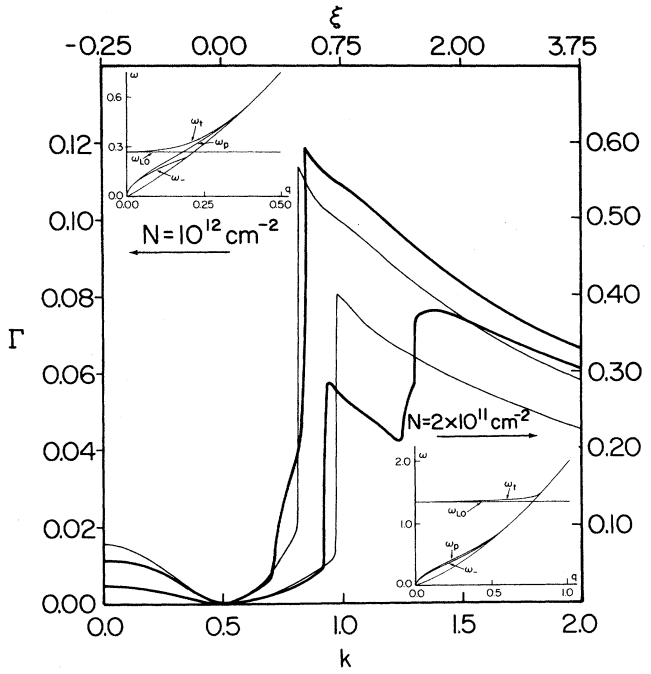

FIG. 8. Damping rate $\Gamma(k)$ for the uncoupled (thin lines) and coupled (thick lines) 2D EG given for two electron densities. The insertions describe the mode coupling in the q-ω plane. The two upper curves, the upper inset, and the vertical scale on the left correspond to $N=10^{12}$ cm^{-2}. The two lower curves, the lower inset, and the vertical scale on the right correspond to $N=2\times10^{11}$ cm^{-2}. Wave vectors are measured in units of $2k_F$; energies and damping rates are measured in units of $4E_F$. On the upper horizontal scale some values of the electron kinetic energy $\xi(k)=k^2-0.25$ are indicated. For $N=2\times10^{11}$ cm^{-2} and $k<0.5$ the coupled and uncoupled results are not distinguishable on the scale of the figure. For $N=10^{12}$ cm^2, $2k_F=5\times10^6$ cm^{-1} and $4E_F=137$ meV; for $N=2\times10^{11}$ cm^{-2}, $2k_F=2.2\times10^6$ cm^{-1} and $4E_F=27.4$ meV.

For the coupled 2DEG the quasiparticle can be scattered either by the excitation of electron-hole pairs or by the emission of a coupled plasmon-phonon (ω_+,ω_-) mode.[22] For low densities the coupling is weak[7] (lower inset in Fig. 8), and the energies of the coupled modes (ω_+ and ω_-) are close to those of the uncoupled ones (ω_{LO} and ω_p). The first step corresponds to the ω_--emission threshold and is located below the k_c of the uncoupled 2D EG because $\omega_-<\omega_p$. The second step corresponds to the ω_+-emission threshold and occurs at a wave vector slightly larger than $(\omega_{\mathrm{LO}}+0.25)^{1/2}$ because $\omega_+>\omega_{\mathrm{LO}}$. For high densities there is a strong coupling(upper inset in Fig. 8), and the threshold for the ω_- emission occurs at a wave vector slightly smaller than $(\omega_{\mathrm{LO}}+0.25)^{1/2}$, which the ω_+-emission threshold is located to the right of the k_c for the corresponding uncoupled 2D EG.

For a given k the damping rate is calculated at the unperturbed energy $\xi(k)$ instead of the quasiparticle energy coming from Dyson's equation. However, the difference between these two energies is small and has no important consequence in the final results. We emphasize that the quasiparticle picture is meaningful over the whole range of wave vectors in Fig. 8. With increasing k the quasiparticle becomes more damped as the thresholds are crossed, but it remains as a well-defined peak of the spectral function.

VI. FINITE-THICKNESS EFFECTS

Until now we have been working in the ideal model of a 2D EG interacting with 3D LO phonons. However, the electrons in a quantum well (QW) are not confined to a 2D plane and their wave functions have a finite width of the order of the well width. This effect weakens the strength of the electron-electron interaction and is usually taken into account[1] by replacing the Coulomb potential V_q by $V_q f_q$, where f_q is the subband form factor. For an infinite square-well potential of width d with only the lowest subband occupied, the form factor is given by

$$f_q=\frac{8}{q^2d^2+4\pi^2}\left[\frac{3}{8}qd+\frac{\pi^2}{qd}-\frac{4\pi^4(1-e^{-qd})}{q^2d^2(q^2d^2+4\pi^2)}\right]. \quad (31)$$

f_q is always smaller than unity and approaches 1 in the small-qd limit. In this section wave vectors q are given in inverse length instead of in units of $2k_F$. The weakening of the Coulomb interaction can be seen in the uncoupled 2D EG by a decrease in the mass correction (Fig. 9) and in the damping rate (Fig. 10) when we go to wider well widths for a given electron density.

The finite thickness of the QW also modifies the LO-phonon spectrum and, consequently, the electron-phonon interaction. A simple approximation which is widely used[6] (3D-phonon approximation) consists of ignoring the change in LO-phonon spectrum and multiplying the Fröhlich coupling constant by the subband form factor (the two-dimensional M_q^2 is replaced by $M_q^2 f_q$). The electron-phonon interaction is then reduced in the same way as the Coulomb interaction. In particular, in the limit of small well widths this approximation reproduces

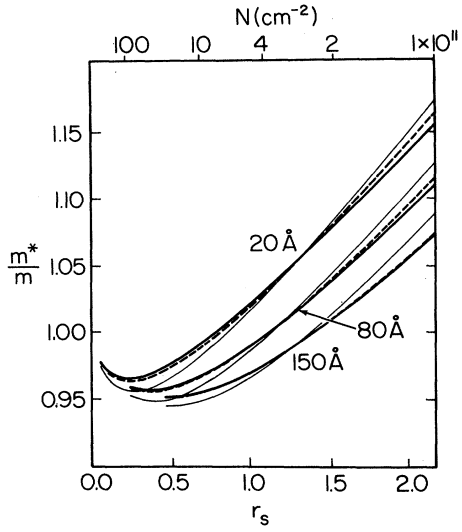

FIG. 9. Effective mass for the quasi-2D EG as a function of the dimensionless interparticle separation parameter r_s for three well widths. Thin solid lines correspond to the uncoupled system, thick solid lines to the coupled system in the 3D-phonon approximation, and thick dashed lines to the coupled system in the slab phonon model. For each well width the maximum electron density shown is that for which the second subband becomes occupied. The units are the same as in Fig. 7.

the model of a 2D EG coupled to 3D LO phonons.

A more realistic approach is to take into account the effects of the confining geometry in the LO-phonon spectrum. This has been the subject of extensive studies.[23–26] Most of these treatments[23,24] rely crucially on the continuum model or the Lorentz relation,[27] which are not valid close (of the order of the lattice constant) to the interfaces. The corresponding results are then valid only in the long-wavelength limit and not for very thin QW's. We will also take this approach and follow Wendler and Pechstedt[24] (WP) in their study of the single quantum well (or double heterostructure), where the LO-phonon spectrum is modified by the inclusion of the bulklike confined slab modes and the interface slab modes (consequently, this is called the slab phonon model). The former ones, which from now on we will refer to as the bulk slab phonons, are confined within the well, and the boundary condition of zero parallel ion displacement at the interfaces gives a quantization condition for their z-component wave vector:

$$q_z^m = \frac{m\pi}{d} , \tag{32}$$

where m is a positive integer and d is the well width. The bulk slab modes are hence discrete and the magnitude of their three-dimensional wave vector $\mathbf{Q}=(\mathbf{q},q_z)$ cannot be smaller than π/d. Ignoring the slight dispersion of the nonconfined LO phonons all the bulk slab phonons are degenerate at ω_{LO}. The bulk slab modes with odd m are symmetric and those with even m are antisymmetric with respect to a reflection about the midplane of the well. The interface slab modes arise from the symmetric and antisymmetric combinations of the individual modes at the two interfaces of the QW. These modes have a slight dispersion, with their energy varying between the LO- and TO-phonon energies of the semiconductors inside and outside the QW. The interface modes decay exponentially as one moves away from the interface according to $\exp(-qz)$, where q is the magnitude of the in-plane wave vector and z is the distance from the interface. Both interface and bulk slab modes have been experimen-

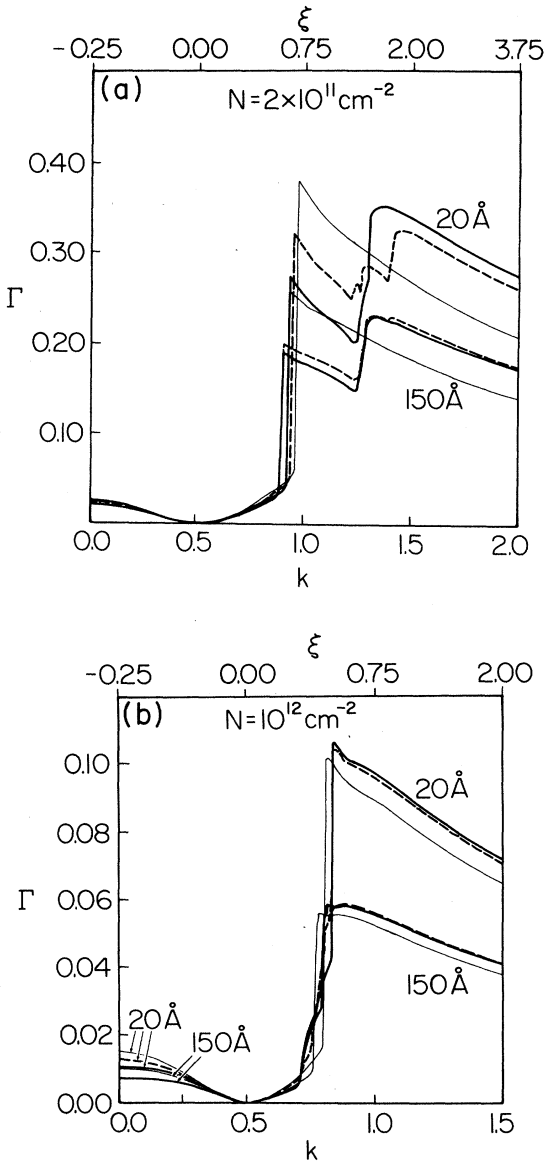

FIG. 10. Damping rate $\Gamma(k)$ of the quasi-2D EG for $N=$ (a) 2×11^{11} cm^{-2} and (b) 10^{12} cm^{-2}. Thin solids lines correspond to the uncoupled system, thick solid lines to the coupled system in the 3D-phonon approximation, and thick dashed lines to the coupled system in the slab phonon model. The units are the same as in Fig. 8. The mean free path is obtained from the dimensionless values k and $\Gamma(k)$ and from the Fermi wave vector $k_F=\sqrt{2\pi N}$ by $l_k=(1/2k_F)[k/\Gamma(k)]$.

tally observed[28] via Raman scattering in thin GaAs quantum wells.

The simultaneous inclusion of the LO-phonon-confining effects beyond the slab phonon model[25,26] and the many-body effects that we have discussed in the preceding sections is a very difficult problem that we will not address in this paper. However, Akera and Ando[26] have recently shown that because of the large gap between the optical branches in the GaAs/AlAs case, the boundary conditions of zero parallel ion displacement at the interfaces are appropriate, indicating the applicability of the slab phonon model in our case. Moreover, the slab phonon model has recently been applied[29] to the problem of hot-electron relaxation in narrow GaAs/$Al_xGa_{1-x}As$ QS's giving a good account of the available experiments.

The Fröhlich coupling of the quasi-2D electrons to the bulk slab phonons is obtained[24] in a similar way as the strictly 2D case, and is given by $M_q^2\beta_q$, where, for the lowest electron subband, the structure factor β_q is given by

$$\beta_q=\sum_{m=1}^{\infty}\beta_q^m , \tag{33}$$

$$\beta_q^m=\begin{cases}\dfrac{256}{\pi^2}\dfrac{qd}{q^2d^2+\pi^2m^2}\dfrac{1}{m^2(4-m^2)^2}, & \text{odd } m \quad (34a)\\ 0, \quad \text{even } m\ . & (34b)\end{cases}$$

Since the electron wave function of the lowest subband is symmetric, the electron-phonon matrix elements (and, consequently, the structure factor β_q) are nonzero only for symmetric modes (odd m). In contrast to the form factor f_q of Eq. (31), β_q vanishes in the small-qd limit instead of approaching unity. Thus, for very thin quantum wells the bulk-slab-phonon results do not reproduce the model of a 2D EG coupled to 3D phonons. β_q^m rapidly decreases with m since the nodes in the ion displacement tend to weaken the coupling strength. The contribution of the $m=3$ mode is already negligible when compared to that of the $m=1$ mode.

The symmetry of the electronic wave function in a symmetric rectangular well indicates that there is coupling only with the symmetric interface phonons (s^+ and s^- modes in WP's notation). Since the dispersion relations $\omega_{s\pm}(q)$ and the coupling constants $M_{q,s\pm}^2$ of the symmetric interfaces modes are rather complicated and since we are closely following WP's notation, we will not elaborate on them in this paper. The properties of the interface phonons depend on the semiconductor inside the QW as well as on the one outside. For the latter we choose $Ga_{0.75}Al_{0.25}As$, whose parameters are $\omega'_{LO}=46.7$ meV, $\epsilon'_\infty=10.2$, and $\epsilon'_0=11.0$.

With the coupling constants M_q^2 of the slab modes, we can again use the formalism of Sec. II to calculate the electron self-energy of the coupled system, the spectral function, the quasiparticle properties, etc. In this section we concentrate on the quasiparticle properties. Figure 9 gives the effective mass as a function of electron density and well width for the uncoupled and coupled quasi 2D EG (the latter calculated in the 3D-phonon approximation as well as taking into account the slab modes). From these graphs we conclude that the main effect of the finite width is a reduction of the Coulomb interaction. Except for very narrow QW's (thinner than 20 Å), the difference between 2D and quasi-2D uncoupled results is always larger than the corrections obtained by the inclusion of the electron-phonon interaction (in any approximation). For wide QW's (thicker than 100 Å), the 3D-phonon approximation gives almost the same results as these with the slab modes. Below 100 Å the 3D-phonon approximation overestimates the phonon correction, and this discrepancy increases as we reduce the well width.

For low densities [Fig. 10(a)] and a very thin (20 Å) QW the damping rate for the slab phonon model (dashed thick lines) is between the results of the uncoupled quasi-2D EG (solid thin lines) and of the coupled quasi-2D EG in the 3D-phonon approximation (solid thick lines), indicating again that the 3D-phonon approximation overestimates the LO-phonon contributions in narrow wells. We point out, however, that for very thin wells the continuum approximation inherent in our theory may break down. In the damping-rate curve of the slab phonon model (Fig. 10) the emission threshold of various modes can be seen: the plasmonlike mode ω_- (between the steps of the uncoupled quasi-2D EG and of the 3D-phonon approximation), the ω_{s-} mode [around $\xi(k)=\omega_{TO}$], the bulk slab modes [around $\xi(k)=\omega_{LO}$], and the ω_{s+} mode [around $\xi(k)=\omega'_{LO}$]. It is important to notice that the scattering of the ω_{s+} mode dominates over the scattering of the bulklike modes. However, the total damping rate is close to that of the 3D-phonon approximation. The necessary conditions for the interface modes to dominate the bulklike ones are thin wells and low electron densities. This is obvious from the fact that the interface modes decay as $\exp(-qz)$ as one moves away from the interface. Thin wells keep z small, while low densities keep k_F, and therefore, the momentum transfer q, small. For a thick QW the 3D-phonon approximation gives results very close to those of the slab phonons. In the damping rate with the slab modes the threshold for the ω_{s+}-mode emission can be seen around $\xi(k)=\omega'_{LO}$.

For high densities [Fig. 10(b)] the 3D-phonon approximation is good for all well thicknesses. The thresholds for the $\omega_{s\pm}$-mode emission, which are below the k_c of the plasmon emission, do not give rise to sharp steps in $\Gamma(k)$ and cannot be easily resolved, as in the low-density case.

For very energetic electrons the mean free path is roughly linear in the kinetic energy ξ. For $N=2\times10^{11}$ cm^{-2} and a well width of 20 Å, taking into account the slab modes, l_k goes from 260 to 470 Å when ξ goes from $2\omega_{LO}$ to $4\omega_{LO}$, while for a 150-Å-thick well the change in the same energy interval is from 390 to 710 Å. For $N=10^{12}$ cm^{-2} in the interval $2\omega_{LO}-4\omega_{LO}$, l_k goes from 180 to 260 Å for a 20-Å-thick well and from 300 to 450 Å in a 150-Å-thick well.

Sawaki[30] has calculated the damping rate in a superlattice and found that the scattering rate is reduced by increasing the well width in the 3D-phonon approximation, and the opposite behavior in the slab phonon model. On the other hand, we always have a reduction of the damping rate by increasing the well width. There are, however, important differences between Sawaki's work and

ours: the former is a one-electron problem, whereas we consider the total damping rate where plasmon and quasiparticle scatterings are very important. Also, the single QW has a different LO-phonon spectrum from that of a superlattice.

Finite-thickness effects do not significantly modify our previous results for the density of states. This is shown in Fig. 11, where the DOS is given for $N=2\times10^{11}$ cm^{-2} and various thicknesses in the 3D-phonon approximation.

VII. CONCLUSIONS

In this paper we have given our calculated results for the low-temperature quasiparticle properties of a GaAs microstructure-based 2D EG taking into account both electron-electron and electron-phonon interaction effects within the leading-order (in the dynamical *effective* interaction) self-energy (both electron and phonon) diagrams. Our results should be directly (and quantitatively) applicable to 2D EG systems in GaAs quantum wells and heterojunctions. Our theory includes all the important dynamical effects including dynamical screening, plasmon-phonon–mode coupling, degeneracy, slab and interface phonon modes, and finite thickness of the electron gas. Even though the theory is only a leading-order (in the *effective* interaction) theory, it should be quite valid in GaAs-based 2D EG because GaAs has very weak Fröhlich coupling and its low effective band mass and high-frequency dielectric constant (ϵ_∞) make the effective r_s parameter quite small. Our theory based on the RPA is exact in the limit of $\alpha\ll1$ and $r_s\ll1$, and, for GaAs, $\alpha=0.07$, whereas $r_s=1.0$ for $N=4\times10^{11}$ cm^{-2}. Our experience from metal physics enables us to trust RPA self-energy results for electron-electron interaction even for $r_s\gtrsim1.0$. On the other hand, α being very small in GaAs, electron-phonon vertex corrections are inherently negligible and our leading-order calculation should be adequate. Thus we speculate that our calculated quasiparticle properties should be quantitatively valid in GaAs down to $N\approx10^{11}$ cm^{-2} ($r_s\approx2$).

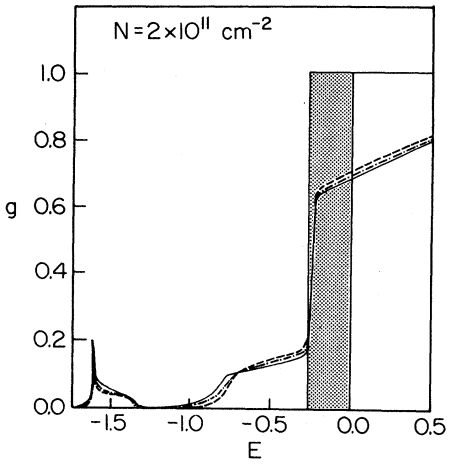

FIG. 11. Density of states for the coupled quasi-2D EG with $N=2\times10^{11}$ cm^{-2} and various well widths (d) in the 3D-phonon approximation. Solid line corresponds to $d=0$. Results for $d=20$ Å cannot be distinguished from those of the 2D EG on the scale of the figure. Dashed-dotted line corresponds to $d=80$ Å and dashed line to $d=150$ Å. The units are the same as in Fig. 6.

An important question is whether the plasmon structure ("plasmaron") and the similar phonon satellite found in our calculated spectral function (and, therefore, in the density of states) is a spurious consequence of our specific approximation scheme. There is no doubt that these structures exist within the RPA used in this paper—plasmarons in a 3D EG have been extensively discussed in the literature.[2] Unfortunately, there is no systematic and controlled approximation scheme for doing calculations beyond the RPA because the diagrams involved [shown as (c) and (d) at the bottom of Fig. 1] are simply intractable. A definitive answer to the question of the existence of these additional spectral structures beyond the RPA, therefore, cannot be provided at the present time. One can, however, convince[2] oneself that the structures exist even if one calculates the self-energy self-consistently, i.e., one uses the fully renormalized Green function G in Eq. (7) instead of G^0. This is done by repeatedly iterating Eq. (7) and the Dyson's equation,

$$G=G^0+G^0\Sigma G\ , \tag{35}$$

simultaneously. Thus diagrams of the sort shown as (c) in Fig. 1 preserve the plasmaron and the phonon satellite structure. Whether vertex corrections [shown as (d), for example, in Fig. 1] wash out these satellite structures or not is not known and is beyond the scope of this study.

We believe that our theoretical results should be *qualitatively* valid in all polar 2D EG systems provided r_s and α are not too large. For stronger electron–LO-phonon coupling there is a problem arising from the unknown contributions made by the vertex corrections. We emphasize that there is *no* Migdal's theorem for polar coupling because electronic and phonon energy scales are comparable (no problem arises from the low dimensionality; however, Migdal's theorem is valid in a 2D EG as long as $\omega_{\rm ph}/E_F$ is very small).

In order to get an idea about how our results would be modified for higher values of polar coupling, we show in Figs. 12 and 13 our calculated numerical results for the quasiparticle spectral function [Eq. (18)] and the effective mass [Eq. (27)] for higher values of the Fröhlich coupling α, keeping all other parameters in the calculation exactly the same as before. We achieve this by suitably adjusting the static dielectric constant ϵ_0 which enters only through the definition of α, and *not* any other parameter of the theory. Thus, even though these results with higher values of α do not correspond to any real material, one can get some idea about trends in quasiparticle properties with an increase in electron-phonon coupling by comparing results in Figs. 12 and 13 with the previous results in this paper (for which $\alpha=0.07$). One can clearly see that various features associated with electron-phonon–coupling effects as discussed earlier are now more accentuated, and results depart even more from the multiplicative renormalization result. With increasing α

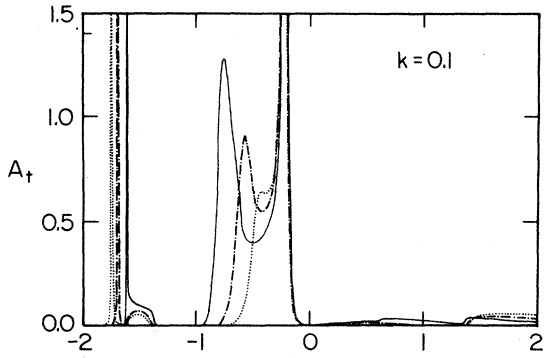

FIG. 12. Spectal function for the coupled 2D EG with $N=2\times10^{11}$ cm^{-2} and various coupling constants (α). Solid line corresponds to $\alpha=0.07$ (appropriate for GaAs), dashed line to $\alpha=0.2$, and dotted line to $\alpha=0.3$. The units are the same as in Fig. 2.

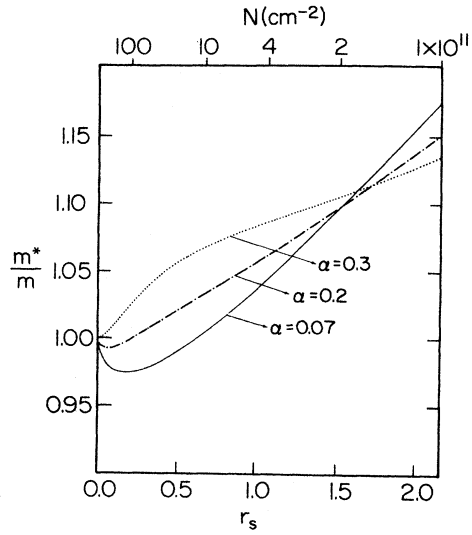

FIG. 13. Effective mass for the coupled 2D EG and various coupling constants (α). The units are the same as in Fig. 7.

the electron structure of the self-energy is reduced with respect to the phonon structure, and the spectral function is dominated by the quasiparticle peak and the peak corresponding to the phononlike solution of the Dyson equation (which moves towards smaller energies with increasing α). We should, however, caution that, for higher α, effects of electron-phonon vertex corrections may very well be significant. We speculate that our results are approximately valid for $\alpha \lesssim 0.25$.

Comparison between our calculated results and experiment is difficult, due mostly to the paucity of relevant experimental results. Most of the effective-mass measurements (e.g., cyclotron resonance, Shubnikov–de Haas) are in the presence of strong magnetic fields and it is not at all clear to what extent a zero-magnetic-field theory is applicable to those situations. Besides the measured phonon-induced effective mass, renormalization in GaAs microstructures is quite small[3] (1% or less) and is totally consistent with our calculated results. We have recently applied[18] this theory to the problem of band-gap renormalization in GaAs quantum wells, and the agreement with experimental results is very good. Finally, some preliminary measurements of *inelastic* mean free path in GaAs microstructures are now available[5] and our theoretical results are consistent with measured values. The structures in which those experiments[5] are carried out are quite complicated and the direct applicability of our theory to these experiments is questionable.

There are a number of predictions in this paper which are, in principle, experimentally testable. Effective mass can be obtained from specific-heat measurements, whereas tunneling studies could give the electronic damping. The interesting structure in the electronic density of states is another experimentally testable feature of the theory.

In summary, we have calculated the quasiparticle properties of a coupled two-dimensional electron–LO-phonon system by treating the Coulomb and Fröhlich interactions on equal footing. Our theory includes the interaction between electrons, LO phonons, and plasmons within the RPA (for dynamical screening and phonon self-energy correction) and within the leading-order self-energy diagram in the *effective total interaction*. Our results should be quantitatively valid for GaAs-based 2D EG in quantum wells and heterojunctions. We find that Coulomb and Fröhlich renormalizations are nonmultiplicative. We also find interesting structure in the calculated density of states that should be experimentally observable. On a general, qualitative level, our results are valid for a 2D EG interacting with Einstein phonons via a long-range interaction.

ACKNOWLEDGMENTS

We would like to thank J. K. Jain and T. Kawamura for careful readings of the manuscript and for valuable suggestions. This work is supported by the United States Army Research Office. We also acknowledge support from the University of Maryland Computing Center.

*Present address: Applied Physics, Yale University, Box 2157, New Haven, Connecticut 06520.

[1]See T. Ando, A. B. Fowler, and F. Stern, Rev. Mod. Phys. **54**, 437 (1982).

[2]L. Hedin and S. Lundqvist, in *Solid State Physics,* edited by H. Ehrenreich, F. Seitz, and D. Turnbull (Academic, New York, 1969), Vol. 23, p. 135; L. Hedin, Phys. Rev. **139**, A796 (1965); B. I. Lundqvist, Phys. Kondens. Mater. **7**, 117 (1967); Phys. Status Solidi **32**, 273 (1969).

[3]U. Merkt *et al.*, Phys. Scr. T **13**, 279 (1986), and references

therein.
[4]T. W. Hickmott *et al.*, Phys. Rev. Lett. **52**, 2053 (1984); P. F. Lu, D. C. Tsui, and H. M. Cox, *ibid.* **54**, 1563 (1985).
[5]J. R. Hayes, A. F. J. Levi, and W. Wiegmann, Phys. Rev. Lett. **54**, 1570 (1985); M. Heiblum *et al.*, *ibid.* **55**, 2200 (1985).
[6]S. Das Sarma, Phys. Rev. B **27**, 2590 (1983); S. Das Sarma and B. A. Mason, Ann. Phys. (N.Y.) **163**, 78 (1985); Phys. Rev. B **31**, 1177 (1985); B. A. Mason and S. Das Sarma, *ibid.* **35**, 3890 (1987); S. Das Sarma, A. Kobayashi, and W. Y. Lai, *ibid.* **36**, 8151 (1987).
[7]X. Wu, F. M. Peeters, and J. T. Devreese, Phys. Status Solidi **133**, 229 (1986); Phys. Rev. B **32**, 6982 (1985); **34**, 2621 (1986).
[8]R. Jalabert and S. Das Sarma, Phys. Rev. B **39**, 5542 (1989).
[9]See, for example, G. Mahan, *Many Particle Physics* (Plenum, New York, 1981).
[10]F. Stern, Phys. Rev. Lett. **18**, 546 (1967); J. K. Jain and P. B. Allen, Phys. Rev. B **32**, 997 (1985).
[11]J. J. Quinn and R. A. Ferrell, Phys. Rev. **112**, 812 (1958).
[12]W. M. McKeeman and L. Tesler, Commun. ACM **6**, 315 (1963); W. Press, B. Flannery, S. Teukolsky, and W. Vetterling, *Numerical Recipes* (Cambridge University Press, London, 1986).
[13]N. D. Mermin, Phys. Rev. B **1**, 2362 (1970).
[14]S. M. Bose *et al.*, Phys. Rev. **155**, 379 (1967).
[15]A. W. Overhauser, Phys. Rev. B **3**, 1888 (1971).
[16]B. Vinter, Phys. Rev. Lett. **35**, 1044 (1975); Phys. Rev. B **13**, 4447 (1976).
[17]G. E. Santoro and G. F. Giuliani, Solid State Commun. **67**, 681 (1988); Phys. Rev. B **37**, 4813 (1988).
[18]S. Das Sarma, R. Jalabert, and S. R. Eric Yang, Phys. Rev. B **39**, 5516 (1989).
[19]M. Jonson, J. Phys. C **9**, 3055 (1976).
[20]T. M. Rice, Ann. Phys. (N.Y.) **31**, 100 (1965).
[21]C. S. Ting, T. K. Lee, and J. J. Quinn, Phys. Rev. Lett. **34**, 870 (1975).
[22]M. E. Kim, A. Das, and S. D. Senturia, Phys. Rev. B **18**, 6890 (1978).
[23]R. Fuchs and K. L. Kliewer, Phys. Rev. **140**, A2076 (1965); A. Lucas, E. Kartheuser, and R. Badro, Phys. Rev. B **2**, 2488 (1970); E. Evans and D. L. Mills, *ibid.* **8**, 4004 (1973); L. Wendler, Phys. Status Solidi B **129**, 513 (1985).
[24]L. Wendler and R. Pechstedt, Phys. Status Solidi B **141**, 129 (1987).
[25]Sung-kit Yip and Yia-Chung Chang, Phys. Rev. B **30**, 7037 (1984).
[26]H. Akera and T. Ando, Phys. Rev. B **39**, 5508 (1989).
[27]See, for example, M. Born and K. Huang, *Dynamical Theory of Crystal Lattices* (Oxford University Press, London, 1966).
[28]A. K. Sood *et al.*, Phys. Rev. Lett. **54**, 2111 (1985); **54**, 2115 (1985).
[29]J. K. Jain and S. Das Sarma, Phys. Rev. Lett. **62**, 2305 (1989).
[30]N. Sawaki, Surf. Sci. **170**, 537 (1986); J. Phys. C **19**, 4965 (1986).